Thermal effects of pyroxenites on mantle melting below mid-ocean ridges / Brunelli, Daniele; Cipriani, Anna; Bonatti, Enrico. - In: NATURE GEOSCIENCE. - ISSN 1752-0908. - 11:7(2018), pp. 520-525. [10.1038/s41561-018-0139-z]

(Article begins on next page)

Melting below Mid Ocean Ridges: thermal effects of pyroxenites in the peridotitic mantle

Daniele Brunelli[1,2*], Anna Cipriani[1,3*], Enrico Bonatti[2,3]

[1] Dipartimento di Scienze Chimiche e Geologiche, Università di Modena e Reggio Emilia, Via Campi 103, 41125 Modena, Italy.

[2] Istituto di Scienze Marine, CNR, Via Gobetti 101, 40129 Bologna, Italy.

[3] Lamont Doherty Earth Observatory, Columbia University, Palisades, New York 10964, USA.

* Corresponding authors: *daniele.brunelli@unimore.it; anna.cipriani@unimore.it*

After travelling in the Earth's interior for up to billions of years, recycled material once injected at subduction zones can reach a subridge melting region as pyroxenite dispersed in the host peridotitic mantle. We studied genetically related crustal basalts and mantle peridotites sampled along an uplifted lithospheric section created at a segment of the Mid Atlantic Ridge through a time interval of 26 Ma. The arrival of low-solidus material into the melting region forces the elemental and isotopic imprint of the residual peridotites and of the basalts to diverge with time. We show that a pyroxenite-bearing source entering the subridge melting region induces undercooling of the host peridotitic mantle, due to subtraction of latent heat by melting of the low-T solidus pyroxenite. Mantle undercooling in turn lowers the thermal boundary layer leading to a deeper cessation of melting. A consequence is to decrease the total amount of extracted melt, hence magmatic crustal thickness. The degree of melting undergone by a homogeneous peridotitic mantle is higher than the degree of melting of the same peridotite but veined by pyroxenites. This effect, thermodynamically predicted for a marble-cake type peridotite-pyroxenite mixed source, implies incomplete homogenisation of recycled material in the convective mantle.

Mantle rising beneath the 60,000 km long Mid Oceanic Ridge system contains, as in a slow-motion movie, a record of ancient upwelling and melting events and of interaction with subduction or hot spot-derived components. It is difficult to reconstruct temporal records of these ancient events due to lack of suitable samples; however, we were given the opportunity to explore the temporal evolution of the oceanic lithosphere composition and structure at 11°N along the Mid Atlantic Ridge (MAR) where an uplifted > 300 km long sliver of lithosphere exposes a basal mantle peridotite unit, lower crustal gabbros, a dyke complex and erupted basalts[1–3]. This lithospheric section (Vema Lithospheric Section or VLS) was generated at an 80 km long segment of the MAR (EMAR segment, Supplementary Fig. S1) during a 26 Ma time interval[1,2,4–6]. Both crustal basalts and their mantle peridotite parents have been densely sampled at the VLS along a seafloor spreading flow line[4] allowing comparisons of their isotopic and elemental composition throughout the 26 Ma time interval[1,2,4–6] (Fig. 1) .

Surprisingly, temporal variations of mantle degree of melting estimated from basalt Na_8[7,8] anti-correlate with the degree of melting derived from spinel Cr# of the peridotites[9,10], although the two curves converge to a common value in the youngest 3 Ma stretch of the VLS (Fig. 1). Older, isotopically enriched basalts display the lower Na_8 values of the entire VLS, suggesting they were generated by a higher degree of melting of their mantle source; in contrast, the genetically associated mantle peridotites record a relatively low extent of melting, in agreement with a thinner crust recorded by geophysical data[1]. This anti-correlation contrasts with what is inferred to be the "normal" signature of partial melting at mid-ocean ridges.

We offer a solution to this conundrum by suggesting that a subridge variably veined mantle hosts chemically enriched, fertile, low-T melting components, i.e. pyroxenites. Thermodynamic-based studies predict dramatic effects when pyroxenites are present in the mantle source and partially melt along a decompressive path[11–15]. Low-T solidus components lower the extent of melting of the host peridotite due to subtraction of latent heat of fusion[13–15]. Pyroxenites melt preferentially, generating isotopically enriched, low Na_8 melts and cooling the host mantle peridotites, thereby lowering the degree of melting of the peridotite mantle in proportion to its pyroxenite content[13]. In this work we account for variable extents of the melting column by assuming that different pyroxenitic contents result in variable extent of undercooling before the ambient peridotite starts melting. This situation mimics varying the potential temperature of the mantle resulting in changes in the length of the melting column.

Temporal variability of crustal thickness and mantle degree of melting

Basalt Nd, Sr and Pb isotopes vary coherently along the 26 Ma-long VLS section, showing a decrease in isotopic enrichment towards younger ages that hints at temporal variations of composition and thermal state of the rising mantle[8]. We represent these variations as discrete steps (Fig. 1a), defining three time domains: 0-2 Ma, 2-13 Ma and 13-26 Ma (Supplementary Tables S1-S3).

The basalts major element composition also varies with age, the older samples being poorer in sodium than the younger ones. Na_8, an inverse proxy of the degree of melting experienced by the mantle column[7,8] (Supplementary Table S2), is on average lower in the VLS older basalts; thus, they were apparently produced by a degree of melting higher than the younger basalts (Supplementary Fig. S1a). However, Na_8 has been defined for a homogeneous lherzolitic source[8]. A heterogeneous source generates complex melt mixing patterns depending on the relative extent of melting, homogenisation and enrichment of each component[16–18]. For this reason we adopt here the expression "apparent" degree of melting.

The proxy equivalent (but reverse) to basalt Na_8 is in peridotites the Cr# (Cr#=Cr/(Cr+Al)) of spinels and pyroxenes[9,10]. During the last 26 Ma, peridotite spinel Cr# increased along the VLS on average from 22 to 37 (Supplementary Fig S1c) suggesting that the amount of magma delivered at ridge axis increased through time, in agreement with gravity profiles running along spreading-flow-lines (Supplementary Fig. S1c), revealing that crustal thickness increased from 4.8±0.2 km in the 22-27 Ma interval to 5.4±0.2 km between 0-5 Ma [1,4].

Based on calibrations of Warren, 2016[19], the degree of melting (F_{max}) of the VLS peridotites increased from 8.0 to 14.2 F% toward younger crustal ages (average 10.8, Fig. 2). MORB glasses Na_8 increased with time along the VLS from 2.6 to 3.0 on average (Supplementary Fig. S1a). F_{max} in the basalts can be estimated according to[7] and compared to the F_{max} of the mantle peridotites. Comparing temporal sections of mantle residua and of their melt products must take into account a time-delay in the emplacement of the mantle peridotites in the oceanic crust. According to[1,4] we corrected the crustal ages of the mantle rocks relative to that of basalts by a relative time lag of 2.2 Ma (see online Methods: Age Correction).

The calculated apparent F_{max} of MORB glasses vary little during the 26 Ma-long VLS stretch (Fig. 1b) with values ranging from 18.0 to 15.8 F% (ave. 16.7), significantly higher than those estimated from mantle residual peridotites (Fig. 1b). A striking feature of the Na_8 degree of melting curve is the decrease of the apparent F_{max} through time that countertrends with both the associated mantle peridotites degree of melting curve and the gravity-inferred crustal thickness (Fig. 1b; Supplementary Fig. S1c).

Significance of the decoupling

The degrees of melting estimated from the mantle peridotites and from the basalts can be generated by variations of mantle potential temperature, mantle composition and spreading rate. Changes in mantle temperature or source fertility will result in coherent changes of the degrees of melting estimated from basalts and from peridotites. Similarly, changes in spreading rate cannot decouple the behaviour of residual mantle and extracted basalts, because, in a passive upwelling scenario, decreasing the spreading rate lowers the thermal state of the entire melting region, and vice versa[20]. During the last 26 Ma the half spreading rate at the EMAR segment decreased from 17.2 mm/a (Chron 6) to 16.9 mm/a (Chron 5) to present-day 13.6 mm/a[21,22] (Supplementary Fig. S1b). Such decrease of spreading rate toward younger ages should lower the mantle degree of melting by about 1%[20]; thus, the increase in degree of melting recorded by the VLS mantle peridotites must be caused by processes other than changes in spreading rate, mantle temperature or fertility.

We consider now a heterogeneous mantle source. Thermodynamic modelling of melting a two-component mantle source predicts that when a fertile heterogeneity, i.e. pyroxenite, starts melting, the temperature of the whole mantle parcel is lowered due to the latent heat of melting[15]. If the heterogeneity is less than a few kilometres, some heat is transferred from the peridotite into the melting heterogeneity increasing its melt productivity while cooling the surrounding mantle[13–15]. Accordingly, the vertical interval where only pyroxenites undergo melting represents an undercooling region whose extent is proportional to the amount of pyroxenites (Fig. 2). It follows that, for a given P-T decompression path, the degree of melting undergone by a homogeneous peridotitic mantle is higher than the degree of melting of the same peridotite but veined by pyroxenites.

A lithologically homogeneous mantle source, resulting in coherent estimates of the degree of melting between peridotites and basalt proxies, is approximated in the younger (< 5 Ma) portion of the VLS where both basalt- and peridotite-derived F% converge toward a common value. We assume that the present-day subridge mantle (Vema Unveined Mantle or VUM) contains negligible amounts of pyroxenites, not sufficient to perturb thermally the melting process of the host mantle peridotite. Thus, for this region the Na_8-derived degree of melting is in line with its original interpretation[7,8,23].

In contrast, in a veined mantle scenario, degrees of melting estimated from peridotites and from basalts differ strongly. While the Cr# records the true F_{max} of the ambient peridotite, the pooled melts aggregate the compositional signal of both (low F) peridotitic and (high F) pyroxenitic melts[18]. We propose that the low degree of melting of the older portion of the VLS peridotites is due to heat consumption during preferential melting of a pyroxenitic component at nearly constant mantle potential temperature. Along the VLS we have decreasing quantities of pyroxenites injected into the melting region, with consequent decrease of the undercooling effect and expansion of the anhydrous peridotite melting region.

We tested this hypothesis by modelling the decompressive adiabatic melting of a mixed source based on the experimental-parameterized algorithm Melt-PX[24]. Mantle potential temperatures have been constrained using the passive flow temperature field model of Bonatti et al., (2003)[1] giving a mantle Tp = 1350 °C. For this temperature and a lherzolitic source containing 15% clinopyroxene, Melt-PX calculations overestimate crustal thickness and mantle degrees of melting observed at the EMAR segment (Fig. 3). These calculations assume that melting ceases at the base of the crust, a boundary condition acceptable for high mantle Tp settings as in fast spreading ridges or hotspots[24,25]. They represent the model maximum allowed thickness at a given thermal setting (Fig. 3). Mantle flow models[1,26] predict the end of melting to occur at $P_f \approx 0.7$ GPa, well below the base of the crust. This condition applies to low-spreading ridges due to heat conduction to the surface resulting in a deep transition from the conductive to the convective thermal region[20,26–28].

As low-melting component we adopted the silica deficient pyroxenite M7-16[29] for reasons defined in the next section. We observe that an increase in the fraction X_p of pyroxenite in the mantle is paralleled by a decrease of degree of melting of the host peridotite (F_π) (Fig. 3) depending also on the final pressure of melting (varying in the range 0.3-1.1 GPa, Fig. 3).

Integration of the melt productivity of the host peridotite and of the pyroxenite along an adiabatic path, weighted by their relative abundance, allows estimating magmatic crustal thickness. Lambart et al., (2016)[24] show that the total magmatic productivity increases proportionally to the amount of pyroxenite in the source. This observation apparently is in contrast with the increase toward younger ages along the VLS of gravity-inferred crustal thickness, paralleled by a decrease of the estimated amount of pyroxenites dispersed within the mantle (Fig. 2, Supplementary Fig. S1c). This contradiction is solved considering that increasing the amount of low-melting lithologies enhances the undercooling of the host peridotitic mantle due to heat diffusion into the melting pyroxenite[13]. Undercooling estimated by Melt-PX calculations can reach up to 40 °C for adiabatic melting under the assumed conditions. Reduced undercooling due to a decrease of the mantle pyroxenite fraction during melting results in shallowing the final pressure of melting from ≈ 1.1 to 0.7 GPa going from the oldest to the youngest VLS sectors (Fig. 3, right panel).

These observations and numerical experiments reveal that in slow-spreading ridges, at constant mantle potential temperature, the arrival of a pulse of pyroxenites in the mantle source region will cause a reduction of crustal thickness. The countertrend of crustal thickness and degree of mantle melting with spreading rate along the VLS is a positive test of our hypothesis.

Composition of the low-solidus component and effects on Na8

The effect of pyroxenite-derived melts on the final composition of the pooled MORB depends upon the nature of the heterogeneities and on their dilution in the peridotite-derived melt[17,30–32]. In mid-ocean ridge settings most pyroxenites produce melts with major-element composition similar to those derived from peridotite[33]. Hence, little reactivity is expected when pyroxenite-derived melts mix with mantle peridotite-derived melts[34]. We thus explore the possible composition of pyroxenites dispersed in the VLS mantle by considering mixing of silica-deficient (SD) and silica-enriched (SE) pyroxenite-derived melts with peridotite-derived melts. In a Na_2O versus MgO diagram, young VLS lavas plot at higher Na_2O content than the older ones (Supplementary Fig. S2). We assume that the youngest VLS Na-rich lavas, i.e. those showing a degree of melting similar to that of the associated peridotites, derive from melting of the VUM source defining a peridotite primitive melt composition that matches the VUM average Na_8 and F% (Supplementary Table S2). We then calculated mixing lines between the VUM primitive melt and pyroxenitic-derived melts obtained experimentally at variable degrees of melting from different sources (Supplementary Fig. S2-S3). Melt mixing affects the estimated Na_8, and consequently the estimated apparent degree of melting, depending on the absolute Na content and Mg/Na ratio of the added melt fraction (Supplementary Fig. S3). Inferred Na_8 and apparent F of the mixed compositions show that SE-derived melts do not reproduce the observed variability for reasonable fractions and degrees of melting of the pyroxenitic-derived components (Supplementary Fig. S3). Among the SD pyroxenites only those having high Mg/Na ratios, as M7-16, match the VLS observed variability. It is worth noting that the mixed melts matching the VLS data are those obtained at high F (F=65%), a value close to those predicted by thermodynamics[13–15]. Based on these calculation the VLS variability can be approximated by linear mixing of a VUM primitive melt with ca. 30% M7-16 type pyroxenite-derived melt.

Size and nature of mantle domains

An important result of thermodynamic modelling[13,14] is that the undercooling inferred from F% decoupling occurs only for a composite source where a lower-T solidus component is finely dispersed in a high-T-solidus host to ensure efficient heat diffusion. Adopting the calibration of [13] for tabular heterogeneities limits their size to be < 1 km, a dimension close to those estimated from seismic scatter (<10 km)[35]. Cryptic stripes of comparable size (4 km) have been described at the SEIR[36] and modelled based on Nd-Hf MORB variability by [37]. The compositional trend observed along the VLS suggests a decreasing decoupling of the measured parameters. The lateral extension of the melting region reaches 300 km in the spreading direction, ca. 70 km along axis[26]. A single large heterogeneity in the older mantle section would have measured tens of km in width, excluding efficient heat diffusion within the heterogeneity itself. We deduce that the older mantle section contained a cluster of small, tabular, low-T solidus components as in Figure 2, decreasing in time from ca. 15% to 0% of the volume.

VLS basalts $^{143}Nd/^{144}Nd$ versus $^{208}Pb/^{206}Pb$ ratios duplicate one of the mixing trends recognized in South Atlantic basalt suites[38,39] (Supplementary Fig. S4), suggesting that those endmembers are ubiquitous in the sub-Atlantic mantle.

VLS glasses $^{143}Nd/^{144}Nd$ and $^{87}Sr/^{86}Sr$ ratios vary in a restricted range (0.51295-0.51317 and 0.70258-0.70351 respectively, Fig. 1, S5, Online Methods); in contrast, mantle peridotite clinopyroxenes display a large scatter ($^{143}Nd/^{144}Nd$: 0.512024-0.513616; $^{87}Sr/^{86}Sr$: 0.702220-0.705508, age corrected values). This different compositional scatter can be generated by chromatographic dispersion in the melting column[40] or through time by reactive melt infiltration and veining[41,42].

The VLS oldest basalts show the highest apparent degree of melting and the most enriched Sr-Nd-Pb isotopic signature (Supplementary Fig. S4-S5). We suggest that their compositions reflect a larger contribution of pyroxenite-derived melts. As a result, the peridotites of the older domain are less affected by decompression melting, and record lower degrees of melting, possibly preserving their original DMM isotopic fingerprint. In contrast, the VLS younger basalts received a negligible contribution of pyroxenite-derived melts. Unfortunately, we do not have enough data on the mantle peridotites of this young VLS stretch because they are still buried below the sea floor; however the few available samples indicate that this parcel of peridotitic mantle underwent high degree of melting.

Distribution of pyroxenites along Mid Ocean Ridges

We attempt now to extend our findings to other portions of the mid ocean ridge system and interpret the chemistry of genetically related basalt/peridotite in terms of the proportion of pyroxenite dispersed in the mantle source. Only two stretches of the global MOR system have basalt-peridotite pairs sampled densely enough to allow first order observations: the northern Mid Atlantic and the Southwest Indian Ridges[19,43]. In both cases along axis mantle peridotites record an extent of melting systematically lower than that recorded by the associated basalts (Fig. 4).

In light of our findings we propose that pyroxenites are widely distributed in subridge mantle sources proportionally to $\Delta F_{\pi}^{\beta} = F_{\beta}^{app} - F_{\pi}$ the difference between the degree of melting derived from basalts and that derived from peridotites (see Online Methods). This interpretation, if correct, should be confirmed by a correlation between the extent of ΔF_{π}^{β} and chemical indicators of the presence of pyroxenite in the source, e.g. the isotopic ratios of radiogenic elements, expected to be enriched in recycled materials. A broad negative correlation appears between the measured ΔF_{π}^{β} and the basalt $^{143}Nd/^{144}Nd$ ratios (Fig. 5, Supplementary Table S4), suggesting the dependence of the Nd isotopic composition on ΔF_{π}^{β} (r^2=0.53) and revealing similar enriching mechanisms in the two ridge systems.

Spreading rate and mantle potential temperature may not be the leading factors affecting the composition of the extracted basalts and of the residual mantle: the relative proportion of pyroxenites versus peridotites in the mantle source maybe more important. A major implication is that at constant temperature a pulse of low-melting pyroxenite entering the melting region may not lead to a pulse of magmatism because the increased undercooling of the mantle shrinks the peridotitic melting region contrasting the increase of instantaneous pyroxenite melt production.

Our results show that low-T melting heterogeneities dispersed in the mantle source affect not only the composition of the extracted basaltic melts, but also the total extent of melting, the volume of extracted melts, and consequently crustal thickness.

Acknowledgments

This work has been supported by Italian-PRIN prot. 2015C5LN35 and by the U.S. National Science Foundation under grant no. OCE-05-51288. We are also grateful for the support of the Deep Energy community of the Carbon Observatory funded by Alfred P. Sloan Foundation. We thank Charlie Langmuir, Henry Dick, Jessica Warren and Monique Seyler, for stimulating insightful discussions and critical reading of an early version of the work. We are grateful to Marco Ligi for his support on geophysics and Sarah Lambart for helping on Melt-PX. We also thank S. Lambart, A. Stracke and an anonymous reviewer for their constructive reviews that greatly improved the manuscript. We are grateful to A. Whitchurch for the editorial assistance. This is Lamont-Doherty contribution number xxx.

Author contributions

D.B. performed the modelling. A.C. analysed the samples. D.B. and A.C. processed the geochemical data and wrote jointly the paper. E.B. provided the opportunity and support for sea-expeditions and work. All the authors discussed the results and the interpretations.

References

1. Bonatti, E. *et al.* Mantle thermal pulses below the Mid-Atlantic Ridge and temporal variations in the formation of oceanic lithosphere. *Nature* **423,** 499–505 (2003).
2. Brunelli, D., Seyler, M., Cipriani, A., Ottolini, L. & Bonatti, E. Discontinuous Melt Extraction and Weak Refertilization of Mantle Peridotites at the Vema Lithospheric Section (Mid-Atlantic Ridge). *J. Petrol.* **47,** 745–771 (2006).
3. Bonatti, E. *et al.* Flexural uplift of a lithospheric slab near the Vema transform (Central Atlantic): Timing and mechanisms. *Earth Planet. Sci. Lett.* **240,** 642–655 (2005).
4. Cipriani, A., Bonatti, E., Brunelli, D. & Ligi, M. 26 million years of mantle upwelling below a segment of the Mid Atlantic Ridge: The Vema Lithospheric Section revisited. *Earth Planet. Sci. Lett.* **285,** 87–95 (2009).
5. Cipriani, A., Brueckner, H. K., Bonatti, E. & Brunelli, D. Oceanic crust generated by elusive parents: Sr and Nd isotopes in basalt-peridotite pairs from the Mid-Atlantic Ridge. *Geology* **32,** 657–660 (2004).
6. Cipriani, A. *et al.* A 19 to 17 Ma amagmatic extension event at the Mid-Atlantic Ridge: Ultramafic mylonites from the Vema Lithospheric Section. *Geochemistry Geophys. Geosystems* **10,** (2009).
7. Plank, T. & Langmuir, C. H. Effects of the melting regime on the composition of the oceanic crust. *J. Geophys. Res.* **97,** 19749–19770 (1992).
8. Klein, E. M. & Langmuir, C. H. Global correlations of ocean ridge basalt chemistry with axial depth and crustal thickness. *J. Geophys. Res.* **92,** 8089 (1987).
9. Dick, H. J. B. & Bullen, T. Chromian spinel as a petrogenetic indicator in abyssal and alpine-type peridotites and spatially associated lavas. *Contrib. to Mineral. Petrol.* **86,** 54–76 (1984).
10. Michael, P. J. & Bonatti, E. Peridotite composition from the North Atlantic: regional and tectonic variations and implications for partial melting. *Earth Planet. Sci. Lett.* **73,** 91–104 (1985).
11. Katz, R. F. & Weatherley, S. M. Consequences of mantle heterogeneity for melt extraction at mid-ocean ridges. *Earth Planet. Sci. Lett.* **335–336,** 226–237 (2012).
12. Weatherley, S. M. & Katz, R. F. Melting and channelized magmatic flow in chemically heterogeneous, upwelling mantle. *Geochemistry Geophys. Geosystems* **13,** Q0AC18 (2012).
13. Katz, R. F. & Rudge, J. F. The energetics of melting fertile heterogeneities within the depleted mantle. *Geochemistry Geophys. Geosystems* **12,** 1–22 (2011).
14. Phipps Morgan, J. Thermodynamics of pressure release melting of a veined plum pudding mantle. *Geochemistry Geophys. Geosystems* **2,** (2001).
15. Sleep, N. H. Tapping of Magmas from Ubiquitous Mantle Heterogeneities : An alternative to Mantle plumes? *J. Geophys. Res.* **89,** 10029–10041 (1984).
16. Ito, G. & Mahoney, J. J. Flow and melting of a heterogeneous mantle: 1. Method and importance to the geochemistry of ocean island and mid-ocean ridge basalts. *Earth Planet. Sci. Lett.* **230,** 29–46 (2005).

17. Shorttle, O. Geochemical variability in MORB controlled by concurrent mixing and crystallisation. *Earth Planet. Sci. Lett.* **424,** 1–14 (2015).
18. Rudge, J. F., Maclennan, J. & Stracke, A. The geochemical consequences of mixing melts from a heterogeneous mantle. *Geochim. Cosmochim. Acta* **114,** 112–143 (2013).
19. Warren, J. M. Global Variations in Abyssal Peridotite Compositions. *Lithos* **248–251,** 193–219 (2016).
20. Bown, J. W. & White, R. S. Variation with spreading rate of oceanic crustal thickness and geochemistry. *Earth Planet. Sci. Lett.* **121,** 435–449 (1994).
21. Cande, S. C., LaBrecque, J. L. & Haxby, W. F. Plate kinematics of the South Atlantic: Chron C34 To Present. *J. Geophys. Res. Solid Earth* **93,** 13479–13492 (1988).
22. Cande, S. C. & Kent, D. V. Revised calibration of the geomagnetic polarity timescale for the Late Cretaceous and Cenozoic. *J. Geophys. Res. Solid Earth* **100,** 6093–6095 (1995).
23. Langmuir, C. H., Klein, E. M. & Plank, T. in *Mantle Flow and Melt Generation at Mid-Ocean Ridges* (ed. Morgan, J. P.) 183–280 (American Geophysical Union, 1992).
24. Lambart, S., Baker, M. B. & Stolper, E. M. The role of pyroxenite in basalt genesis: Melt-PX, a melting parameterization for mantle pyroxenites between 0.9 and 5 GPa. *J. Geophys. Res. Solid Earth* **121,** 0–28 (2016).
25. Shorttle, O. & Maclennan, J. Compositional trends of Icelandic basalts: Implications for short-length scale lithological heterogeneity in mantle plumes. *Geochemistry, Geophys. Geosystems* **12,** (2011).
26. Ligi, M., Cuffaro, M., Chierici, F. & Calafato, A. Three-dimensional passive mantle flow beneath mid-ocean ridges: an analytical approach. *Geophys. J. Int.* **175,** 783–805 (2008).
27. Mckenzie, D. & Bickle, M. J. The volume and composition of melt generated by extension of the lithosphere. *J. Petrol.* **29,** 625–679 (1988).
28. Shen, Y. & Forsyth, D. W. Geochemical constraints on initial and final depths of melting beneath mid-ocean ridges. *J. Geophys. Res.* **100,** 2211–2237 (1995).
29. Lambart, S., Laporte, D. & Schiano, P. Markers of the pyroxenite contribution in the major-element compositions of oceanic basalts: Review of the experimental constraints. *Lithos* **160–161,** 14–36 (2013).
30. Stracke, A., Bourdon, B. & McKenzie, D. Melt extraction in the Earth's mantle: Constraints from U-Th-Pa-Ra studies in oceanic basalts. *Earth Planet. Sci. Lett.* **244,** 97–112 (2006).
31. Stracke, A. & Bourdon, B. The importance of melt extraction for tracing mantle heterogeneity. *Geochim. Cosmochim. Acta* **73,** 218–238 (2009).
32. Rubin, K. H., Sinton, J. M., Maclennan, J. & Hellebrand, E. Magmatic filtering of mantle compositions at mid-ocean-ridge volcanoes. *Nat. Geosci.* **2,** 321–328 (2009).
33. Lambart, S., Laporte, D. & Schiano, P. An experimental study of pyroxenite partial melts at 1 and 1.5GPa: Implications for the major-element composition of Mid-Ocean Ridge Basalts. *Earth Planet. Sci. Lett.* **288,** 335–347 (2009).
34. Lambart, S., Laporte, D., Provost, a. & Schiano, P. Fate of Pyroxenite-derived Melts in the Peridotitic Mantle: Thermodynamic and Experimental Constraints. *J. Petrol.* **53,** 451–476 (2012).
35. Helffrich, G. R. & Wood, B. J. The Earth's mantle. *Nature* **412,** 501–7 (2001).

36. Graham, D. W., Blichert-Toft, J., Russo, C. J., Rubin, K. H. & Albarede, F. Cryptic striations in the upper mantle revealed by hafnium isotopes in southeast Indian ridge basalts. *Nature* **440,** 199–202 (2006).
37. Liu, B. & Liang, Y. The prevalence of kilometer-scale heterogeneity in the source region of MORB upper mantle. 1–8 (2017).
38. Hoernle, K. *et al.* On- and off-axis chemical heterogeneities along the South Atlantic Mid-Ocean-Ridge (5-11°S): Shallow or deep recycling of ocean crust and/or intraplate volcanism? *Earth Planet. Sci. Lett.* **306,** 86–97 (2011).
39. Paulick, H., Münker, C. & Schuth, S. The influence of small-scale mantle heterogeneities on Mid-Ocean Ridge volcanism: Evidence from the southern Mid-Atlantic Ridge (7°30′S to 11°30′S) and Ascension Island. *Earth Planet. Sci. Lett.* **296,** 299–310 (2010).
40. Liang, Y. Simple models for dynamic melting in an upwelling heterogeneous mantle column: Analytical solutions. *Geochim. Cosmochim. Acta* **72,** 3804–3821 (2008).
41. Borghini, G. *et al.* Meter-scale Nd isotopic heterogeneity in pyroxenite-bearing Ligurian peridotites encompasses global-scale upper mantle variability. *Geology* **41,** 1055–1058 (2013).
42. Borghini, G. *et al.* Pyroxenite Layers in the Northern Apennines' Upper Mantle (Italy)—Generation by Pyroxenite Melting and Melt Infiltration. *J. Petrol.* **57,** 625–653 (2016).
43. Gale, A., Langmuir, C. H. & Dalton, C. A. The global systematics of ocean ridge basalts and their origin. *J. Petrol.* **55,** 1051–1082 (2014).

Figure captions

Figure 1: Figure 1. a) Temporal variation of the VLS basaltic glasses $^{143}Nd/^{144}Nd$ isotopic ratios. Solid circles define three domains (average Nd isotopic ratio of each sector is indicated). Dashed line is average of oldest sector without one enriched sample.

b) Temporal variation of the degree of melting as inferred by mantle peridotite residues[19] and erupted MORBs[7]. Each point represents a dredge average. Thick bold lines are linear regressions; thin lines show 95% confidence bands. The age of mantle rocks is corrected for the time lag between their arrival at the seafloor and the arrival of the basaltic melts they produced according to [1,4] (see Methods).

Figure 2: Interpretative sketch of the upwelling mantle column below the Vema Lithospheric Section. At constant mantle potential temperature the presence of pyroxenites causes a contraction of the melting region. Total degree of decompressive adiabatic melting is computed based on Melt-PX algorithm[24]. In the older VLS sectors, the onset of melting of the mantle peridotite is delayed and its degree of melting reduced (F_{max}=8). The associated pyroxenite melts more (F_{max}=53) and contributes to the higher apparent degree of melting in the pooled MORBs. Undercooling of the mantle peridotite causes deepening of the end of the melting column estimated to shallow by 0.4 GPa from the older to the younger sector.

Figure 3: Melt-PX[24] numerical experiments for adiabatic melting of a two-component mantle source: lherzolite plus SD pyroxenite (M7-16[29]). The thick black line represents the model limit value for melting ceasing at the base of the crust.

Left Panel: the degree of melting of the host peridotite is lowered by adding up to 40% pyroxenite in the source. Variable extents of the melting column are computed assuming P_f from 1.1 to 0.3 GPa. Red dashed lines correspond to the VLS average melting interval from old (F_{max}=8.0) to young (F_{max}=14.2) sectors.

Panel B: Variation of the aggregated crustal thickness as function of pyroxenite fraction in the source and final depth of melting. Average values for the VLS extremes are plotted as red symbols and 1σ standard deviation

Figure 4: Variation of the degree of melting estimated from mantle peridotite (blue dots) and associated basalts (red dots) along the Southwest Indian Ridge (upper) and the Mid Atlantic Ridge from the Equator to the Azores hotspot region (lower). Degrees of melting are calculated based on [19,23,43] on data compiled from PetDB (www.earthchem.org/petdb). Variations of the amount of low-T melting heterogeneities (pyroxenite) in the source result in larger differences in the estimated degree of melting (ΔF_{π}^{β}), a proxy for the along axis pyroxenite vol% content of the source.

Figure 5: Difference of degree of melting estimated from genetically related basalts and peridotites (ΔF) versus the Nd isotopic composition of basalt. The VLS sectors are plotted as large red circles; delta F increases from sector 1 to 3 (young to old). Black diamonds represent SWIR, blue circles MAR. Regression lines are calculated for the whole population (red solid line), the SWIR (black solid line) and the MAR (blue solid line). Data and parameters in supplementary Table S4; 95% confidence bands are plotted in Supplementary Fig. S6. Our interpretation is that the ΔF between basalt and peridotite is a proxy of the amount of low-T solidus pyroxenites in the source.

METHODS

Analytical Methods

Major elements

Major elements on mineral phases were collected with the electron probe (Cameca SX100) at the American Museum of Natural History (NY) using 15kV acceleration voltage, 20nA beam, a 10µm diameter beam and 30 s counting times. Sodium, potassium and chlorine were run under different conditions to attain a higher precision and monitor their mobility, with a 5nA beam and counting times of 80 s. A subset of samples has been analyses with a Cameca X-Five microprobe at the CAMPARIS micro-analytical center (University of Paris VI), following procedures detailed in [44]. A number of primary mineral standards were used, as well as the MORB JDF-D2 standard.

Isotope ratios

For isotopic determinations 50 to 250 mg of basaltic glass and clinopyroxene separate were prepared by grinding, sieving and handpicking under a binocular microscope. Glass chips were leached in 8N HNO_3. Clinopyroxenes were treated with three leachates to eliminate the effects of seawater alteration[5,45]. Pb was separated using AG1-X8 anion resin, Sr was separated using Eichrom Sr resin and Nd was separated in a two-column procedure using Eichrom TRU-spec resin to separate the rare-earth elements, followed by α-hydroxy isobutyric acid. Isotopes were measured on a VG Sector 54 multicollector mass spectrometer housed at the Lamont Doherty Earth Observatory of Columbia University. Sr and Nd isotopes were measured in multidynamic mode. The mass fractionation corrections were based on $^{86}Sr/^{88}Sr$ = 0.1194 and $^{146}Nd/^{144}Nd$ = 0.7219. Over the period of analytical work, repeated analyses yielded a $^{87}Sr/^{86}Sr$ ratio of 0.710271 ± 0.000015 for the NBS-987 Sr standard (2σ external reproducibility, n>22) and a $^{143}Nd/^{144}Nd$ ratio of 0.512096 ± 0.000023 for the JNdi-1 (2σ external reproducibility, n>38). Total blanks for Sr and Nd did not exceed 80pg. Pb data on basaltic glasses were collected in static mode, using the double spike technique with the calibrated 207/204 spike. Replicate analyses of the Pb isotope standard NBS981 gave an average of 16.9317±0.0022 and 15.4912±0.0027 and 36.7060±0.0066 for $^{206}Pb/^{204}Pb$, $^{207}Pb/^{204}Pb$, and $^{208}Pb/^{204}Pb$, respectively. These measured Pb isotope ratios were corrected to the values defined by [46] of 16.9356, 15.4891, and 36.7006, respectively, for NBS 981. Reproducibility for NBS981 is 130, 174, and 181 ppm (2σ, N=47), for $^{206}Pb/^{204}Pb$, $^{207}Pb/^{204}Pb$, and $^{208}Pb/^{204}Pb$ ratios, respectively. Pb blanks measured were below 100pg and thus negligible relative to the amount of sample analysed.

Estimate of the ΔF_{π}^{β} and $^{143}Nd/^{144}Nd$ of the associated basalts

Figure 4 of the main text reports the correlation between ΔF_{π}^{β}, as the differential in degree of melting between basalt and peridotites, and the Nd isotopic composition of basalts of several portions of the Mid Ocean Ridge system where both basalts and peridotites have been sampled. Among all the explored ridge segments, only few localities report basalts and mantle peridotites sampled in the same dredge haul or site. Basaltic rocks are generally more abundant and present a much denser lateral sampling than mantle peridotites. Basalt chemistry and isotopic ratios appear to vary systematically over variable length scale defining domains in which they show little variability or monotonic changes along the ridge axis (e.g. [43, 47-48] among others). Domains characterized by reduced variability of the chemical character of the basalts are usually bounded by major transform faults, which also act as thermal barriers[47,49-51]. Therefore, in Figure 4 (main text), we have chosen to integrate the dataset of the sites where peridotites and basalts were sampled together with sites where only mantle rocks were recovered, but for which is possible to infer the isotopic composition of the associated basalts from the regional variability. As a conservative approach, we only considered those domains in which lateral isotopic and compositional variability is very low or described by simple monotonic trends.

The degree of melting of mantle-peridotites can be affected by Cr# fluctuations due to melt/rock interaction that modify spinel[9] and pyroxene compositions[52]. Therefore we filtered spinel composition and applied a threshold of TiO_2<0.15 wt% as discussed in [2,19]. The supplementary Table S4, reports the inferred values showing the measured and calculated value for each basalt-peridotite couple. The "regional regression" data are calculated considering sets of neighboring peridotites and basalts, whereas the "local average" set of data refers to basalts and peridotites sampled from the same site. ±σ on ΔF_{π}^{β} are estimated by error propagation.

Age correction

Basalts from the VLS were erupted over a time range of 26 Ma. We applied, hence, an age correction for radiogenic ingrowth since the closure of the system to allow comparisons of their initial isotopic composition, which is controlled only by the source. The correction time should be calculated since the closure of the system, represented by the moment of separation between the source and the melt at depth, assuming there was no significant melt-rock interaction thereafter. This is attested by mantle residual rocks from the VLS being all equilibrated in the spinel field showing no late interaction with melts. The only report of plagioclase-equilibrated mantle rocks concerns the strain-driven formation of plagioclase in fertile lherzolites during mylonitization[53]. We identify the melt-source separation at the estimated upper limit of melting as inferred by modelling with Melt-PX (see main text).

Based on the estimation of melting a composite source and varying the position of the end of the melting column between 1.2 and 0.3 GPa, it appears that the end of the melting column can be constrained based on the correlation with the measured crustal thickness and degree of melting of the residual mantle. For the time stretch relative to the VLS the end of the melting column can be set at 1.1 GPa for the older domain and 0.7 GPa for the younger domain. Based on Africa-South America Euler vectors of [21] and the geomagnetic time scale of [22], the spreading rate at the EMAR axis can be estimated through time. As shown in Figure 1 of the main text, the spreading rate decreased steadily in the last 30 Ma. The absolute value decreases from 17.2 to 16.9 mm/y at Chron 6 (half spreading rate) and from 16.9 to 13.6 mm/y at Chron 5. Crustal ages can be calculated accordingly during this time stretch assuming basalts erupted in the axial region.

Times of extraction for the mantle residue and for the basalts are, however, very different. Ascent rates for the basaltic liquids are estimated in the range of m/y [54-56]. Setting the melt/source separation at 1.1 and 0.7 GPa and upwelling rates in the range 1-5 m/y [56] gives upwelling times ranging 7-36 ka for the older VLS domain and 5-23 ka for the younger VLS domain. Such delays are uninfluential in the age correction of long-time decay systems as those here discussed (Sm-Nd; Rb-Sr; U-Pb); however, we considered this contribution for the total age correction when discussing age corrected values in Figs 1B and S1.

Upwelling of the mantle lasts a significant amount of time and can sensibly modify the isotopic relationships. The time necessary for a mantle parcel to join the crust from the end of melting depth is 2.1 Ma for the older VLS domain and 1.7 Ma for the younger VLS domain.

References

44. Seyler, M. & Brunelli, D. Sodium□chromium covariation in residual clinopyroxenes from abyssal peridotites sampled in the 43°–46°E region of the Southwest Indian Ridge. *Lithos* **302–303,** 142–157 (2018).
45. Cipriani, A., Bonatti, E. & Carlson, R. W. Nonchondritic ^{142}Nd in suboceanic mantle peridotites. *Geochemistry, Geophys. Geosystems* **12,** 1–8 (2011).
46. Todt, W., Cliff, R., Hanser, A. & Hofmann, A. W. Evaluation of a 202Pb–205Pb double spike for high - precision lead isotope analysis. *Geophys. Monogr. Ser.* **95,** 429–437 (1996).
47. Meyzen, C. M. *et al.* New insights into the origin and distribution of the DUPAL isotope anomaly in the Indian Ocean mantle from MORB of the Southwest Indian Ridge. *Geochem. Geophys. Geosyst.* **6,** Q11K11 (2005).
48. Meyzen, C. M., Toplis, M. J., Humler, E., Ludden, J. N. & Mevel, C. A discontinuity in mantle composition beneath the southwest Indian ridge. *Nature* **421,** 731–733 (2003).
49. Cannat, M., Rommevaux-Jestin, C., Sauter, D., Deplus, C. & Mendel, V. Formation of the axial relief at the very slow spreading Southwest Indian Ridge (49° to 69°E). *J. Geophys. Res.* **104,** 22825–22843 (1999).
50. Seyler, M., Brunelli, D., Toplis, M. J. & Mével, C. Multiscale chemical heterogeneities beneath the eastern Southwest Indian Ridge (52°E-68°E): Trace element compositions of along-axis dredged peridotites. *Geochemistry, Geophys. Geosystems* **12,** (2012).
51. Paquet, M., Cannat, M., Brunelli, D., Hamelin, C. & Humler, E. Effect of melt/mantle interactions on MORB chemistry at the easternmost Southwest Indian Ridge (61°–67°E). *Geochemistry, Geophys. Geosystems* **17,** (2016).
52. Brunelli, D., Paganelli, E. & Seyler, M. Percolation of enriched melts during incremental open-system melting in the spinel field: A REE approach to abyssal peridotites from the Southwest Indian Ridge. *Geochim. Cosmochim. Acta* **127,** 190–203 (2014).
53. Cannat, M. & Seyler, M. Transform tectonics, metamorphic plagioclase and amphibolitization in ultramafic rocks of the Vema transform fault (Atlantic Ocean). *Earth Planet. Sci. Lett.* **133,** 283–298 (1995).
54. Spiegelman, M. & Kenyon, P. The requirements for chemical disequilibrium during magma migration. *Earth Planet. Sci. Lett.* **109,** 611–620 (1992).
55. Spiegelman, M. & Elliott, T. Consequences of melt transport for uranium series disequilibrium in young lavas. *Earth Planet. Sci. Lett.* **118,** 1–20 (1993).
56. Lundstrom, C. C., Gill, J., Williams, Q. & Perfit, M. R. Mantle Melting and Basalt Extraction by Equilibrium Porous Flow. *Science (80-.).* **270,** 1958 LP-1961 (1995).

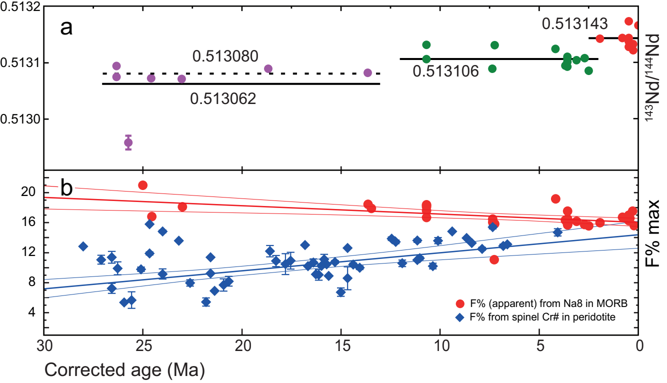

0.5132
0.5131
0.5130
a
0.513080
0.513062
0.513106
0.513143
143Nd/144Nd
b
20
16
12
8
4
F% max
F% (apparent) from Na8 in MORB
F% from spinel Cr# in peridotite
30
25
20
15
10
5
0
Corrected age (Ma)

Fig. 1

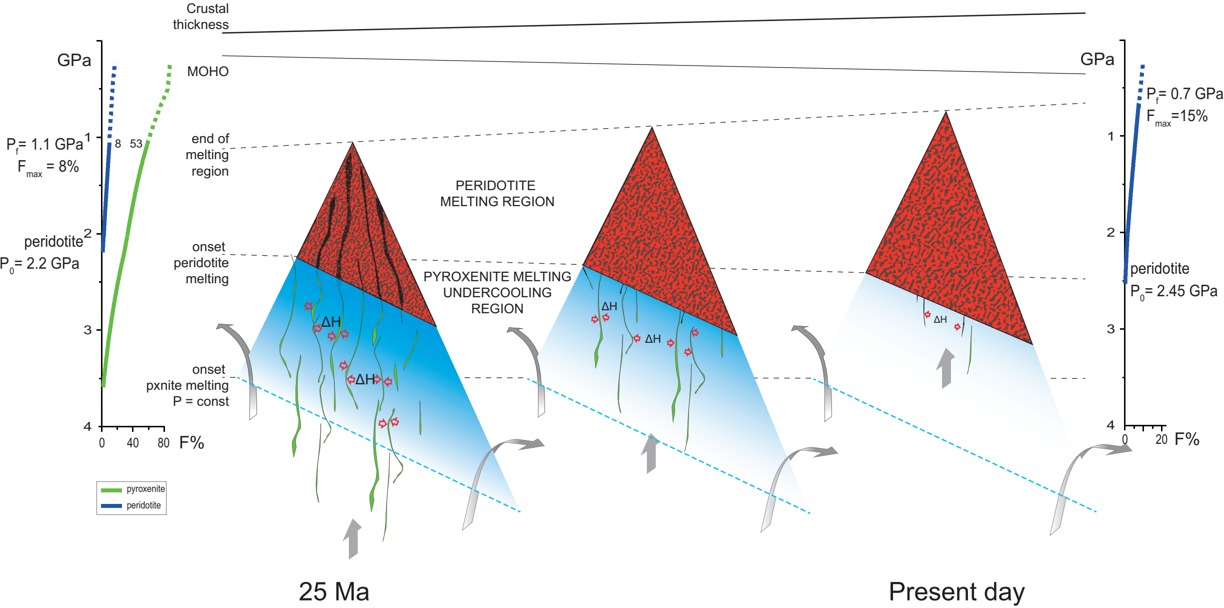

Figure 2 - last

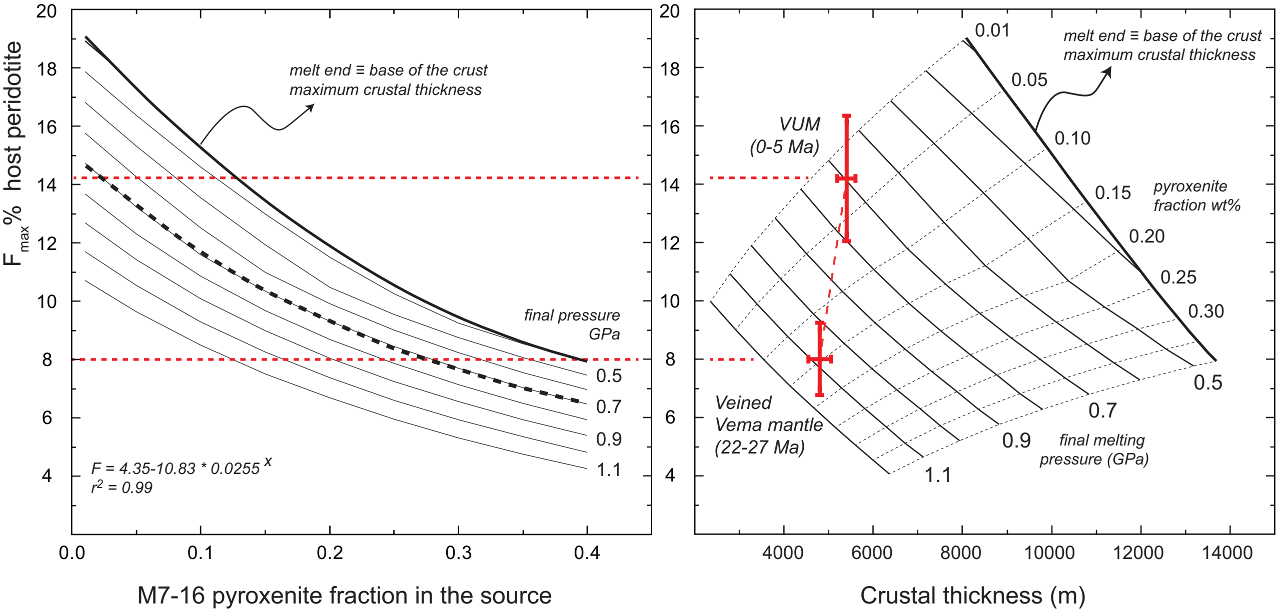

Figure 3_last

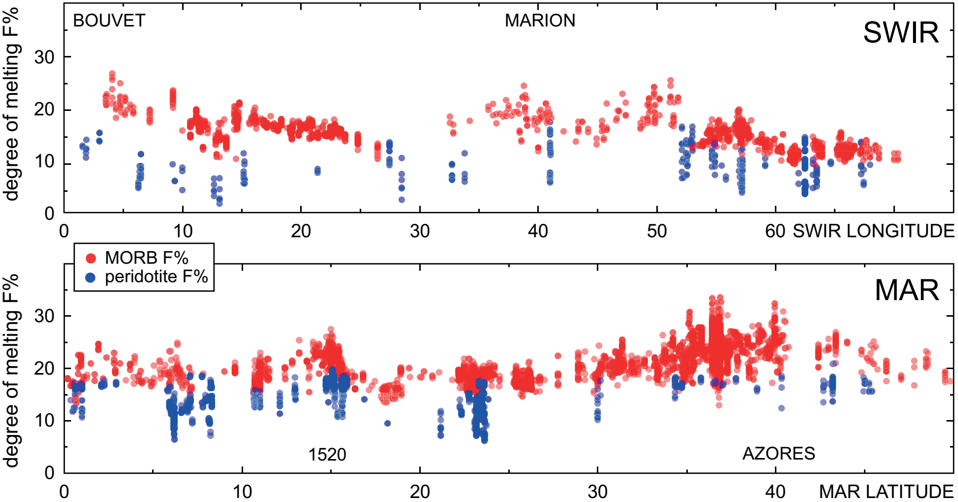

Figure 4-last

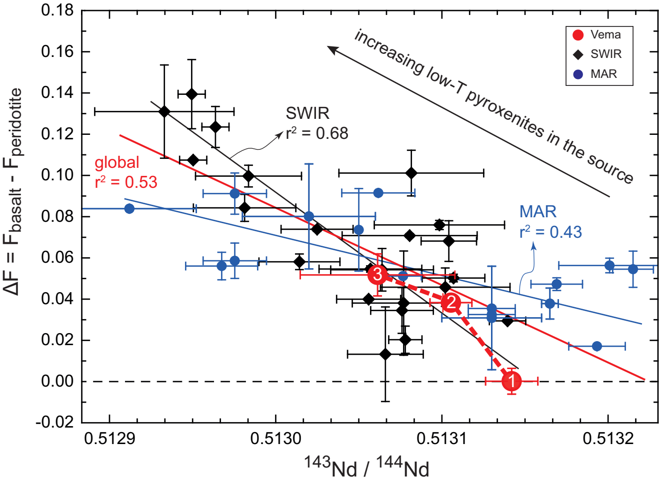

Figure 5 - last